# Measurement of Neuropeptide Y using Aptamer-Modified Microelectrodes by Electrochemical Impedance Spectroscopy

*Luis López*[a], *Nerika Hernández*[a], *Joshua Reyes Morales*[a], *John Cruz*[a], *Krystal Flores*[a], *John González-Amoretti*[a], *Vitmary Rivera*[a], *Lisandro Cunci*[a,*]

[a]Department of Chemistry, Universidad Ana G. Méndez, Carr. 189, Km 3.3, Gurabo, Puerto Rico 00778, United States

## Corresponding Author

* Tel.: +1-787-743-7979 x9-4744; fax: +1-787-743-4114; E-mail address: cuncil1@uagm.edu (L. Cunci).

SUPPLEMENTAL INFORMATION

**Table of Contents**

## Electrochemical Characterization

Previous work has been reported that modifications of the surface increase the signal detection of biomolecules[1]. The use of single-stranded DNA aptamers allows not only the increase of the detection of the molecule of interest, but also decreases non-specific adsorptions to the microelectrodes surface[2]. Therefore, changes in the electrochemical properties of the surface were studied before and after the modifications of the surface on Pt and carbon-fiber. Both, carbon fiber (Figure S1 A-C) and platinum microelectrodes (Figure S1 D-F) were studied to understand the changes produced by the aptamer on the electrochemistry of the surface. Figure S1A and Figure S1D show scanning electron microscopy (SEM) images of carbon fiber and platinum microelectrodes, respectively, as prepared before electrochemical experiments. As can be seen in Figure S1B and Figure S1E, in the cyclic voltammetry performed to carbon fiber and platinum microelectrodes, respectively, the modification of the microelectrodes changed the redox reaction in both materials, as well as the reversibility of the reaction observed by the changes in the difference between the oxidation and reduction peaks. Moreover, EIS was employed to study the chemical changes of the surface of the aptamer-modified microelectrodes. Figure S1C shows the EIS of carbon-fiber microelectrodes oxidized (CF bare) and after the crosslinking reaction with the NPY-targeted DNA aptamers (CF/Aptamer) in 5 mM $K_3FeCN_6/K_4FeCN_6$. Figure S1F shows the EIS of platinum microelectrodes bare (Pt bare), modified with thioglycolic acid (Pt/TGA), and after the crosslinking between thioglycolic acid and the NPY-targeted DNA aptamers (Pt/TGA/Aptamer). EIS is a powerful analysis technique to detect the changes in the interfacial properties of the electrode and the interaction of analytes with their probing molecules immobilized on electrode surfaces[3]. In the case of carbon-fiber microelectrodes, a decrease was seen in the electrical currents of the redox reaction and its reversibility given by the increased separation between the oxidation and reduction peaks due to the aptamer modification. These results are seen in the voltammograms shown in Figure S1B and Figure S1E, and they are consistent also with the data obtained using EIS where $R_{ct}$ increases with the aptamer modification from 327,700 to 491,400 Ohms and from 571,900 to 712,100 Ohms as seen in Figure S1C where two time constants are seen related to the redox reaction since none of these appear in aCSF without the redox couple. This in turn is contrary to the behavior seen in Pt microelectrodes with the aptamer modification. The modification of the platinum microelectrodes with TGA decreases the electrical current of the reduction and oxidation reactions and separates their peaks showing a decrease in the reversibility of the reaction. This may be due to an increase in the difficulty produced by the presence of TGA in the transfer of electrons, which was confirmed by the EIS seen in Figure S1F where $R_{ct}$ increased with TGA almost six-fold (from 133,900 to 788,400 Ohms). Moreover, the latter modification with aptamers increases again the oxidation and reduction electrical currents as well as improves its reversibility moving the peaks closer together even though they are still ca. 110 mV apart. This result is confirmed by the decrease of the $R_{ct}$ with the presence of the aptamer from 788,400 to 11,490 Ohms as seen in Figure S1F. This change has been seen before with the modification of metal surfaces with single-stranded DNA[4].

An explanation of this behavior is due to the interaction that the aptamer has with Pt microelectrodes where it produces a decrease in the charge transfer resistance due to the easier electron transfer from the platinum to the solution through the negatively charged DNA aptamer which should be solvated due to the high concentration of ions in aCSF. This allowed the interaction between the aptamer and $FeCN_6^{-3}/FeCN_6^{-2}$. In the case of the carbon fiber microelectrodes, the carbodiimide crosslinking reaction changes

the carboxyl groups to an amide and prohibits the charge transfers through these previously carboxyl functional groups decreasing the active area where the electron transfer has a lower activation energy. Therefore, a bigger fraction of the surface area has $sp^2$ carbon structure with a higher activation energy for the electron transfer to a charged redox couple.

Information contained in the EIS at higher frequencies (higher than ca. 500 kHz) is attributed to the conductivity of the electrolyte solution involved in the electrochemical reaction, impedance at middle frequencies (typically between ca. 100 Hz and 500 kHz) is usually highly impacted by the charge transfer resistance and double layer capacitance, and low frequencies (less than ca. 10 Hz) are associated with mass transport limitation. In Figure S1F, Nyquist plots present a linear relationship between the Z'' (imaginary component of the impedance) and Z' (real component of the impedance) at low frequency (starting at 252.4 Hz for Pt Bare, 125.6 Hz for Pt/TGA, and 2.528 kHz for Pt/TGA/Aptamer), indicating a diffusion process, which is typical of the $K_3FeCN_6/K_4FeCN_6$ redox couple in platinum[5]. Moreover, this diffusion process was confirmed when plotting the anodic and cathodic peak currents versus the square root of the scanning speed as can be seen in Figure S4 obtaining a linear relationship. However, this phenomenon was not observed in carbon-fiber microelectrodes (Figure S1C) showing that at 0.2 V vs Ag|AgCl the redox reaction was not limited by diffusion due to the low kinetics found using carbon-fibers with this redox reaction[6]. These results show again the improvement typically found in electron transfer when using Pt instead of carbon-fiber microelectrodes. We could take advantage of the electrochemical properties of Pt if we were able to improve the biofouling produced by biomolecules in its surface at least to the level of the biofouling found in carbon fibers.

## Physical Characterization

Scanning electron microscopy (JEOL JSM-6010LA) was used to observe the surface of the microelectrode, while the energy dispersive X-ray spectra (EDS) were obtained to see changes in composition of the surface of the microelectrodes.

## Surface Characterization

SEM images shows the length, integrity, and the structure of the surface of the carbon fiber (Figure S1A) and platinum (Figure S1D) microelectrodes. Figure S1A shows a carbon-fiber microelectrode trimmed using a razor blade with the of the exposed carbon-fiber tip labeled. Figure S1D shows an image of the platinum wire structure of the surface after the fabrication process which elongates the originally 25 µm fiber until ductile breakage where the width ends up being ca. 16 µm. While SEM images showed a good seal between the materials and the glass, water was used to test to what extent the seal was formed and that the solution was not going to be able to enter by capillary action and change the electroactive area of the microelectrodes during experimentation. Fabrication of the microelectrodes was reproducible using the developed method for platinum and carbon-fiber microelectrodes explained in the Experimental Section, although their length may vary within the specified range due to the different ductility of platinum compared to carbon fiber which makes their fabrication done by pulling/breaking instead of having to razor cut the fiber. In these images, a carbon fiber of 7 um of diameter and ca. 100 um length, and a platinum microelectrode of 16.7 um width and 56.16 um length are shown.

**Surface Modification of Microelectrodes**

Energy-dispersive X-Ray spectroscopy (EDS) was used to characterize and observe the integrity of the fabrication and composition of the microelectrodes as well as the surface modifications. An electron accelerating energy of 20 keV was used to obtain the spectra, which is why they are shown up to 10 keV. Figure S2A and Figure S2B show the spectra of carbon fiber microelectrodes before and after their electrochemical oxidation, respectively. Two peaks can be clearly seen in the spectra at 0.28 and 0.53 keV for carbon and oxygen, respectively. The oxygen peaks confirmed the presence of carbon-oxygen moieties. Figure S2C shows the spectrum after aptamer immobilization where an increase in oxygen content is clearly seen due to the surface modification. Figure S2D, Figure S2E, and Figure S2F show the spectra of a platinum microelectrodes before surface modification, after TGA immobilization, and after aptamer tethering, respectively. The peaks seen at 0.28, 0.39, 0.53, 1.49, 1.58, 2.05, 2.13, 8.04, and 9.44 keV correspond to the carbon $K\alpha_1$, Nitrogen $K\alpha_1$, oxygen $K\alpha_1$, aluminum $K\alpha_1$, aluminum $K\beta_1$, platinum $M\alpha_1$, platinum $M\beta_1$, copper $K\alpha_1$, and platinum $L\alpha_1$ peaks, respectively. The peaks that correspond to aluminum and copper appear due to the sample holder behind the tip. After TGA immobilization (Figure S2E), we see an increase in the amount of oxygen at the surface of the platinum microelectrode, which is reduced again after the aptamer tethering (Figure S2F) where the amount of nitrogen is seen increased.

The results observed using EDS to characterize the surface modification are aligned with what was explained above using EIS, where each surface modification produces a change in the surface electrochemical behavior. Moreover, we have seen much more change in EIS compared to EDS, due to the high sensitivity of electrochemical impedance measurements as a surface characterization technique.

Figure S3 shows the cyclic voltammetry of platinum microelectrodes before and after electrochemical pretreatment. While the initial cyclic voltammetry after the platinum breakage shows defined peaks at -0.08 V and 0.00 V vs Ag|AgCl that corresponded to (110) and (100) planes, after the electrochemical pretreatment, the movement of the peaks to higher voltage suggests the change in surface morphology to having more terraces and less defined planes[6].

Surface modification of metal electrodes with self-assembled monolayers typically requires a roughness factor of less than 1.5[7–10] which is impossible in this kind of electrode due to the needle-shaped form factor. Therefore, a monolayer is not possible; however, thiol-ended molecules can still be used to cover the surface of the microelectrodes to decrease the biofouling even though it cannot be completely covered. In order to test the extent to which the biofouling compares to carbon fibers, we modified the microelectrodes as explained in the Experimental Section.

The oxidation of the surface of the carbon fiber microelectrodes was seen by the appearance of the redox peaks for the quinone/hydroquinone reaction on the graphitic surface. As reported in the literature, this electrooxidation produces the formation of carboxyl groups at the surface of the electrodes that can be used to attach amine-ended aptamers using carbodiimide crosslinking reactions[11]. In the case of platinum, thioglycolic acid was used to have the carboxyl group on the surface for aptamer immobilization. While there are different ways to produce similar modifications on the surface of metal electrodes like directly using a thiol-terminated aptamer, we have seen that the use of an intermediate step of thioglycolic acid adsorption to the surface of the microelectrode resulted in several advantages. For example, it allows for

a better coverage of the surface, more versatility in the adsorption reaction, and provides an intermediate step where we can probe the surface using electrochemical techniques to better understand the changes that we are producing in the surface for the microelectrodes[4]. After the last reaction, aptamers should be immobilized in the surface of the microelectrodes. In order to confirm this reaction, several characterizations techniques were used.

Cyclic voltammetry (CV) of these bare and modified microelectrodes were performed using the redox probe containing 5 mM $K_3FeCN_6/K_4FeCN_6$ which was recorded at different scanning speeds, 500, 200, 100, 50, and 20 mV/s. Electrochemical characterization using cyclic voltammetry of both materials is shown in Figure S4. Cyclic voltammetry of carbon fiber and platinum microelectrodes at the different stages of surface modification shows the expected behavior according to their size. Carbon fiber microelectrodes are made of a fiber that is 7 µm thick and less than 100 µm long, which behaves as a classical ultramicroelectrode showing a steady state electrical current at the scanning speeds that were used due to the small size. Platinum, on the other hand, having a bigger size of about 20 µm thick and about 70 µm long, shows a behavior that resembles less an ultramicroelectrode with a significant change in electrical current at different scanning speeds. At room temperature, scanning speeds of about 1 mV/s or less would be required to measure the steady state electrical current of platinum microelectrodes.

**Electrochemical Impedance Characterization of the Aptamers on Carbon Fiber and Platinum Microelectrodes**

To understand the effect of the surface modification on the microelectrodes, we also used EIS with an amplitude of 10 mV and a frequency range from 10 Hz to 5 MHz. shows Figure S7A EIS Bode plots of the platinum and carbon-fiber microelectrodes in 5 mM $K_3FeCN_6/K_4FeCN_6$ solution at potentials from -0.4 to 0.4 V and from -0.6 to 0.2 V vs Ag|AgCl, respectively. The potentials for platinum were chosen in a way that we can observe positive and negative charges without going as far as the hydrogen evolution. Additionally, the potentials for carbon fiber microelectrodes were chosen at potentials where biomolecules do not oxidize and polymerize at the electrode surface in addition to 0.2 V which is the $E_{1/2}$ potential for the redox couple used in these experiments. Bode plots shown display two time constants at the $E_{1/2}$ potential (0.2 V vs Ag|AgCl), thus, confirming that even though there is only one redox process through the electrode-solution interface in $K_3FeCN_6/K_4FeCN_6$, the surface of the microelectrodes has structural inhomogeneities producing different areas with dissimilar difficulties for the electron transfer[2,12]. Moreover, higher resistance was seen in platinum microelectrodes (Figure S7B) at higher frequencies after the surface modification. However, this phenomenon was not observed in carbon microelectrodes (Figure S7A), which may have been due to the placement of the microelectrodes at the electrochemical cell since the impedance at high energies measures the solution resistance between the working and reference electrodes.

It has been reported that aptamer modifications of electrodes improve the sensitivity and the selectivity of the detection of neuropeptides[13,14]. In order to see the effect of NPY adsorption to the surface, we used cyclic voltammetry at different scanning speeds, 500, 200, 100, 50 and 20 mV/s, in platinum microelectrodes with aptamers (Figure S7C) with and (Figure S7D) without the presence of 500 ng/mL NPY. Changes in the electrochemical response of the platinum surface was observed, which was related to the adsorption of NPY to the aptamers at the microelectrodes. The microelectrode surface increases

the electrical current seen in the voltammograms which is due to the change in capacitance of the surface observed by the width of the cyclic voltammetry. This data agrees with our previous results showing the affinity of NPY with aptamer-modified platinum microelectrodes.

Figure S8 shows the EIS of different NPY concentrations at different potentials in aptamer-modified carbon microelectrodes to show the comparison with platinum microelectrodes that are shown in Figure 3 of the main article.

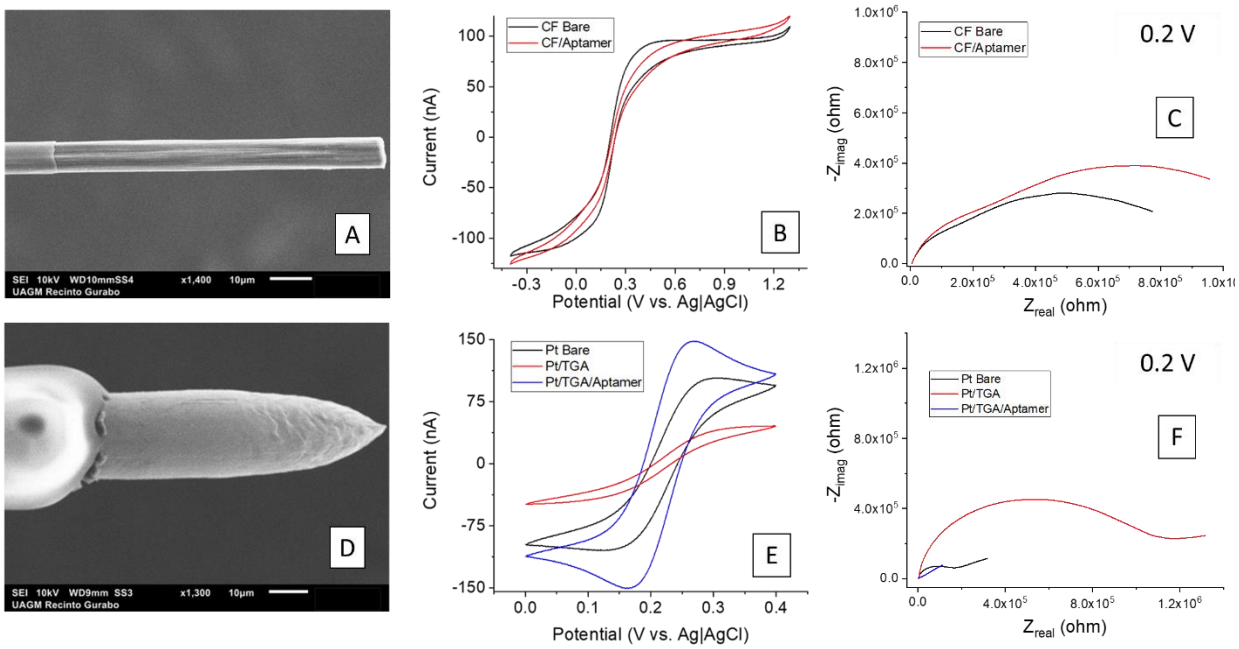


Figure S1 – Characterization of (A-C) carbon fiber and (D-F) platinum microelectrodes by (A, D) scanning electron microscopy images, (B, E) cyclic voltammetry, and (C, F) electrochemical impedance spectroscopy. Cyclic voltammetry was done at 200 mV/s and all electrochemical experiments were done in a 5 mM $K_3FeCN_6/K_4FeCN_6$ solution in aCSF buffer.

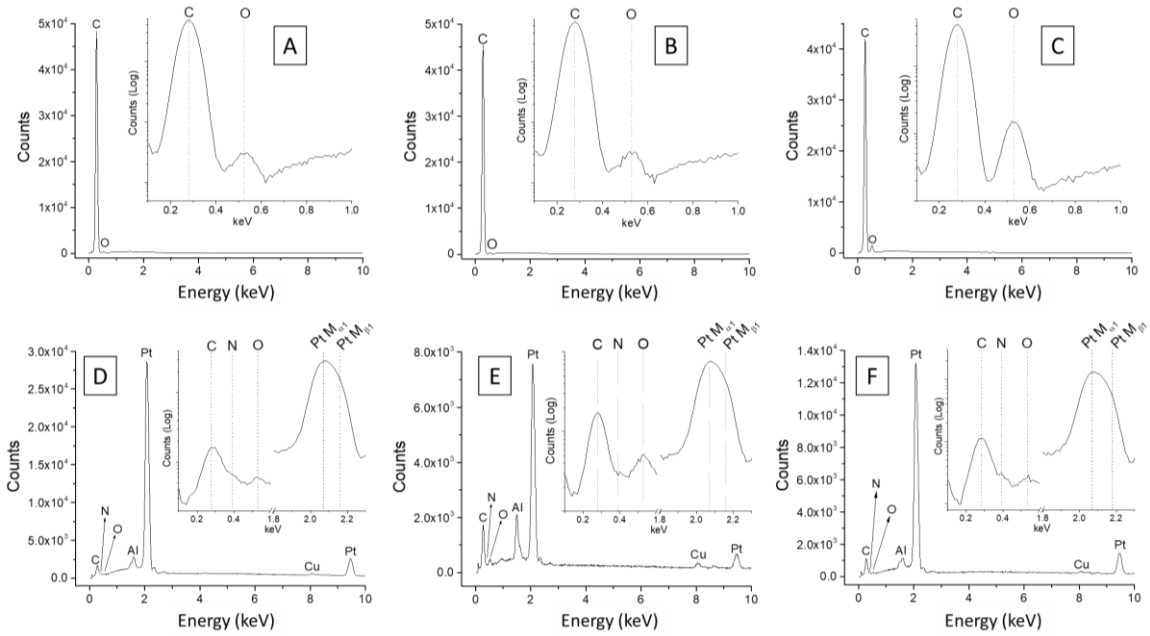


Figure S2 – Characterization of the surface modifications of (A-C) carbon fiber and (D-F) platinum microelectrodes using energy-dispersive X-ray spectroscopy with accelerating voltage of 20 kV. A through C show the spectra of carbon fiber microelectrodes (A) before and (B) after oxidation, and (C) after aptamer immobilization. D through F show the spectra of platinum microelectrodes (D) before and (E) after TGA and (F) aptamer modifications.

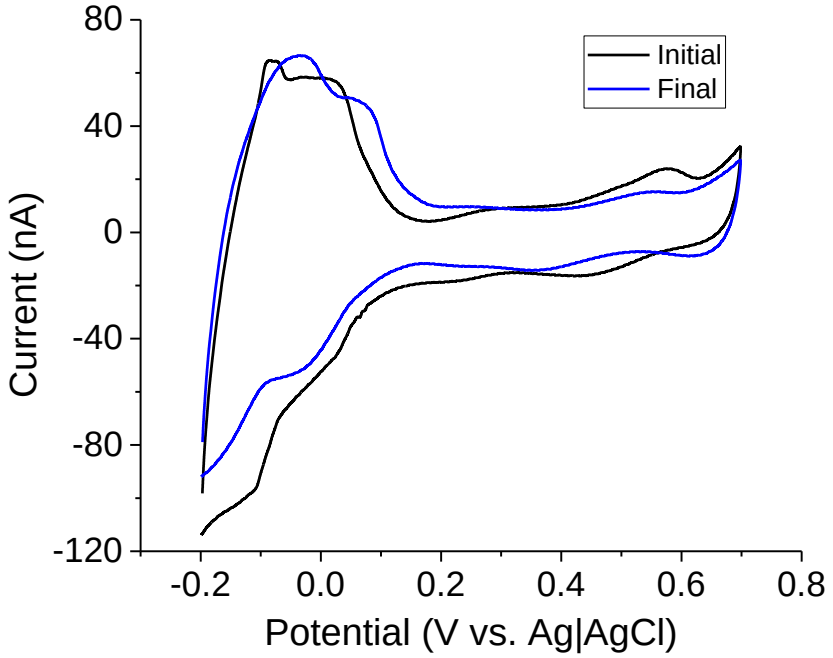


Figure S3 – Cyclic voltammetry of a platinum microelectrode before (Initial) and after (Final) 300 cycles at 100 mV/s in 0.5 M $H_2SO_4$. 0.02 V are (100) planes and terraces.

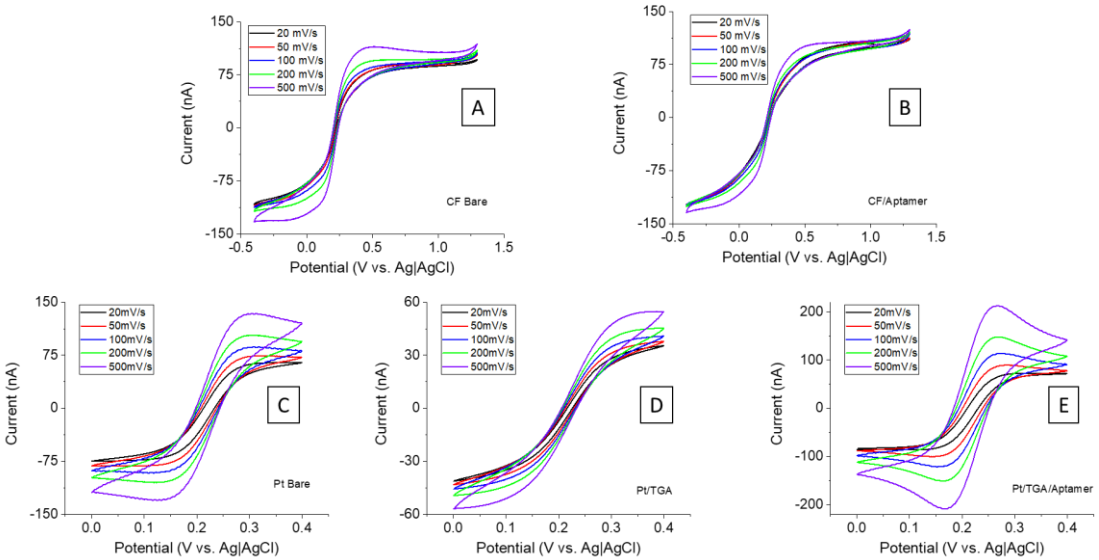


Figure S4 – Cyclic voltammetry of (A) bare and (B) aptamer-modified carbon fiber, and (C) bare, (D) TGA-modified, and (E) Aptamer-TGA-modified platinum microelectrodes at different scanning speeds specified in the legend of each plot. All cyclic voltammetry experiments were done in a 5 mM $K_3FeCN_6/K_4FeCN_6$ solution in aCSF buffer.

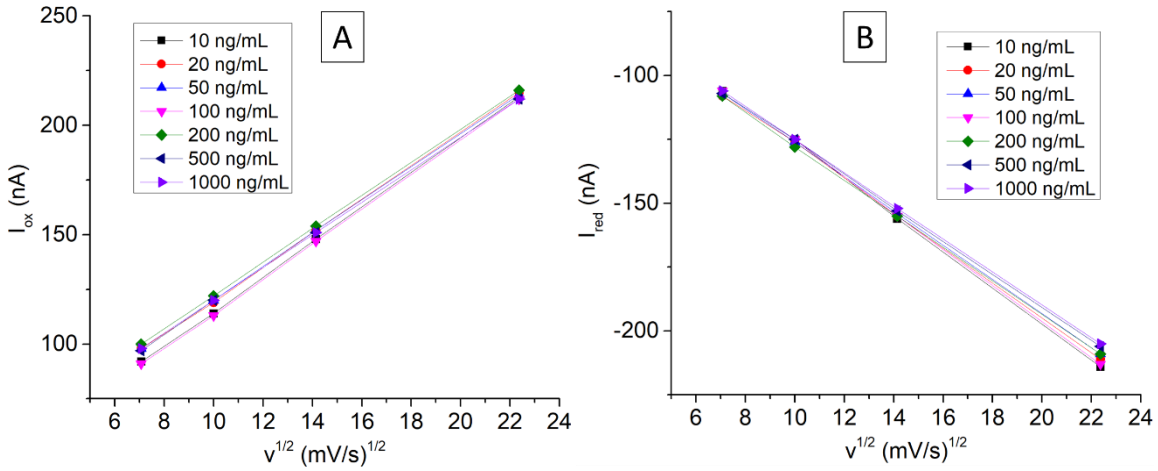


Figure S5 – (A) Anodic peak current, $I_{ox}$, and (B) cathodic peak current, $I_{red}$, versus $v^{1/2}$. All experiments were run in a 5 mM $K_3FeCN_6/K_4FeCN_6$ solution in aCSF buffer.

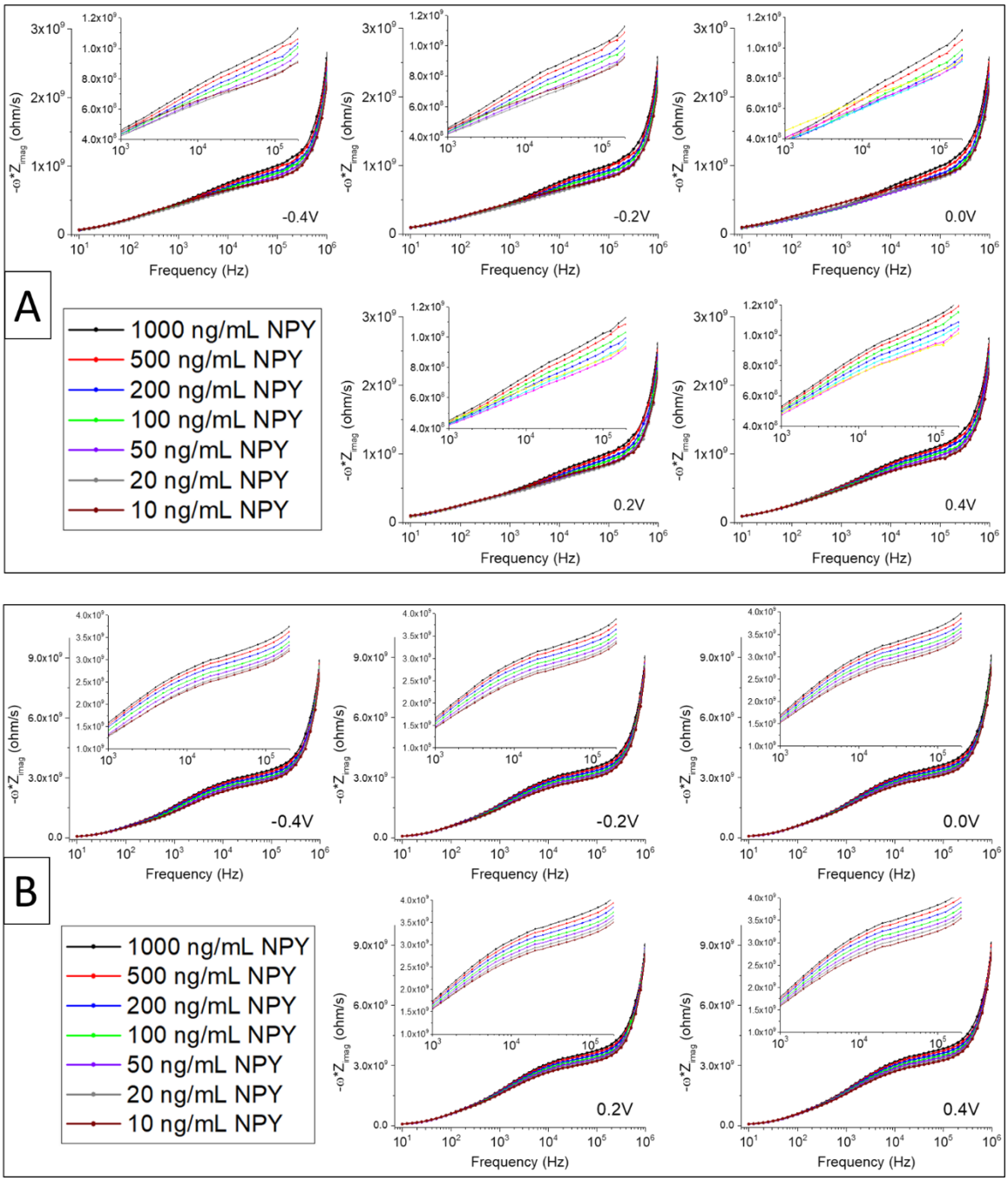


Figure S6 – Electrochemical impedance spectroscopy ($-\omega * Z_{imag}$) of different NPY concentrations at different potentials in (A) bare and (B) aptamer-modified platinum microelectrodes.

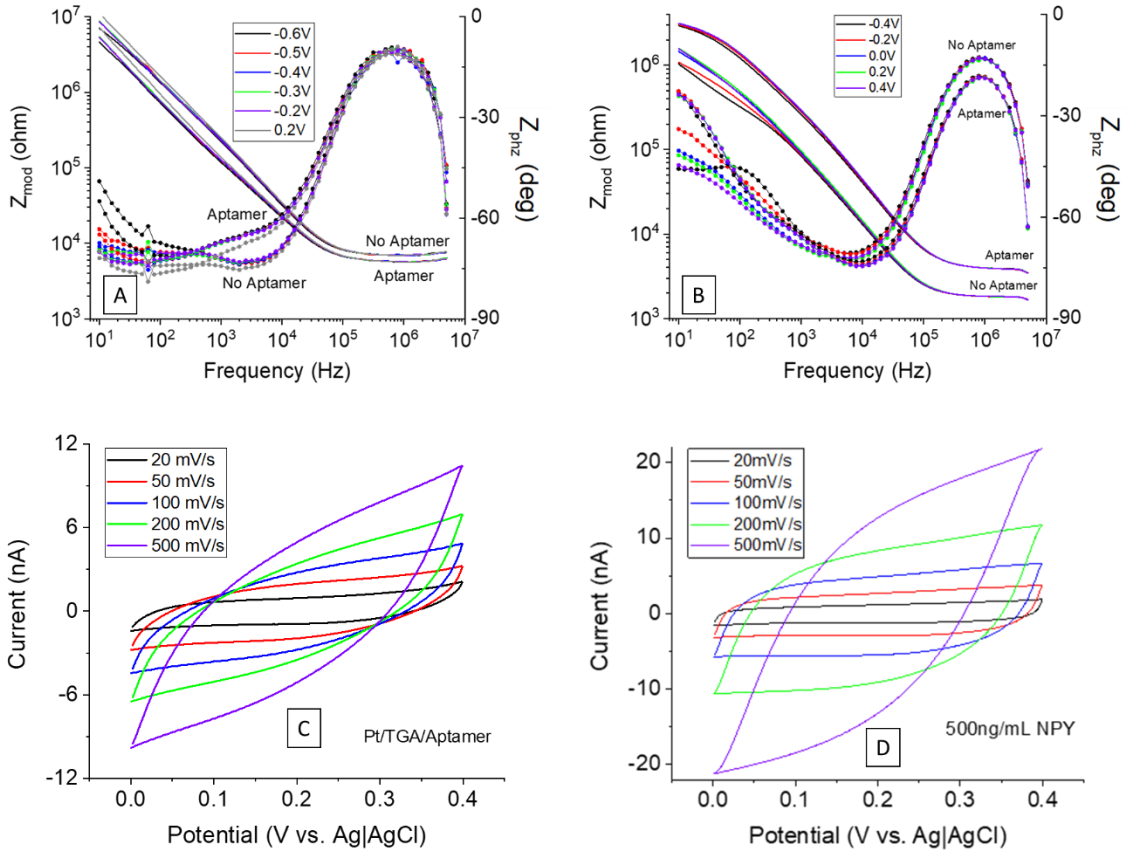


Figure S7 – Effect of the aptamer modification on (A) carbon fiber and (B) platinum microelectrodes in the surface seen using electrochemical impedance spectroscopy at different potentials. Cyclic voltammetry of aptamer-modified platinum microelectrode (C) before and (D) after NPY adsorption. The cyclic voltammetry experiments were done at different scanning speeds specified in the legend of each plot with 500 ng/ml of NPY in aCSF buffer.

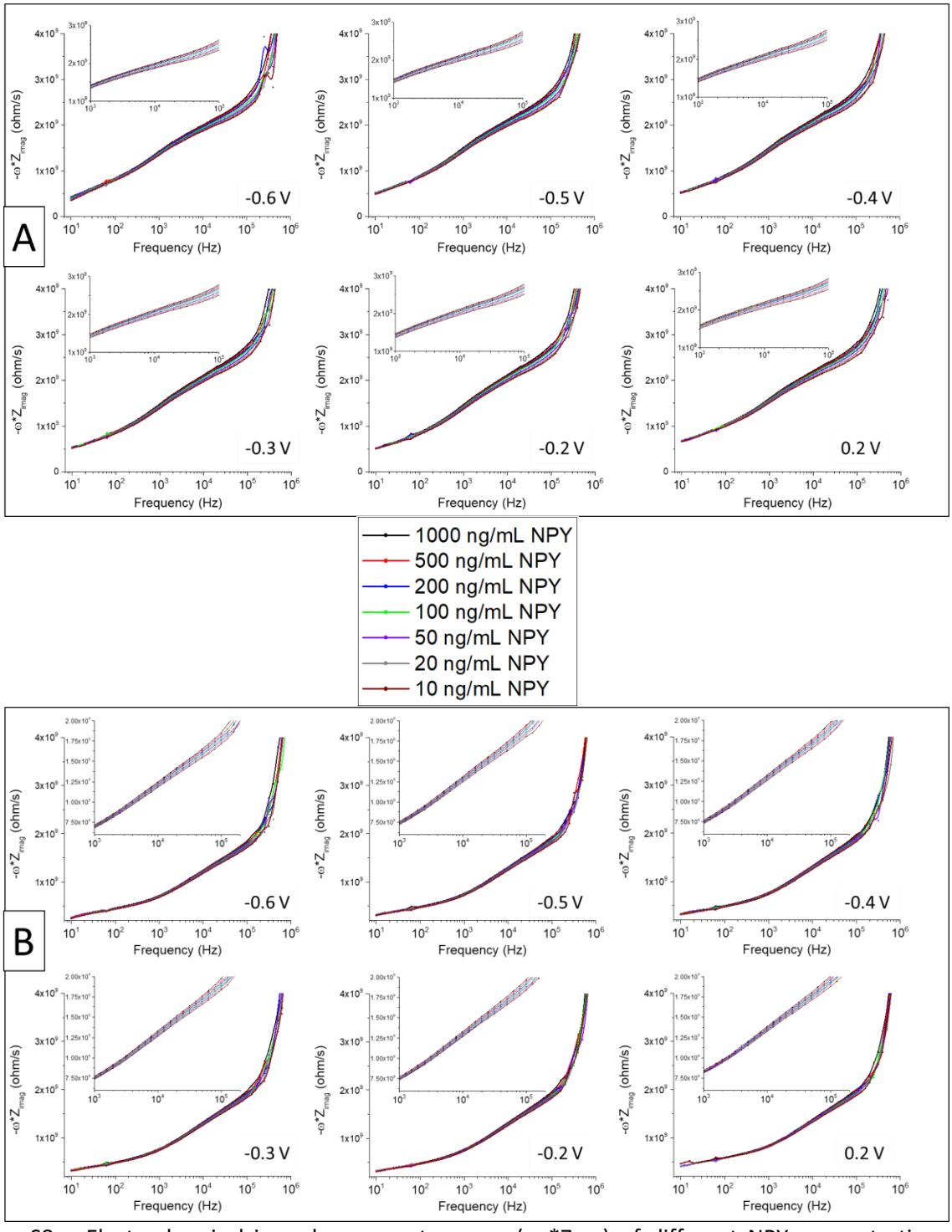


Figure S8 – Electrochemical impedance spectroscopy ($-\omega*Z_{imag}$) of different NPY concentrations at different potentials in (A) bare and (B) aptamer-modified carbon microelectrodes vs. Ag|AgCl in aCSF buffer.

**References**


(1) Jiang, L.; Nelson, G. W.; Abda, J.; Foord, J. S. Novel Modifications to Carbon-Based Electrodes to Improve the Electrochemical Detection of Dopamine. *ACS Appl. Mater. Interfaces* **2016**, *8* (42), 28338–28348.

(2) Bai, H.-Y. Y.; Campo, F. J. del; Tsai, Y.-C. C. Sensitive Electrochemical Thrombin Aptasensor Based on Gold Disk Microelectrode Arrays. *Biosens. Bioelectron.* **2013**, *42* (1), 17–22.

(3) Randviir, E. P.; Banks, C. E. Electrochemical Impedance Spectroscopy: An Overview of Bioanalytical Applications. *Anal. Methods* **2013**, *5* (5), 1098.

(4) Cunci, L.; Martinez Vargas, M.; Cunci, R.; Gomez-Moreno, R.; Perez, I.; Baerga-Ortiz, A.; Gonzalez, C. I.; Cabrera, C. R.; Vargas, M. M.; Cunci, R.; Gomez-Moreno, R.; Perez, I.; Baerga-Ortiz, A.; Gonzalez, C. I.; Cabrera, C. R. Real-Time Detection of Telomerase Activity in Cancer Cells Using a Label-Free Electrochemical Impedimetric Biosensing Microchip. *RSC Adv.* **2014**, *4* (94), 52357–52365.

(5) İsbir-Turan, A. A.; Üstündağ, Z.; Solak, A. O.; Kılıç, E.; Avseven, A. Electrochemical and Spectroscopic Characterization of a Benzo[c]Cinnoline Electrografted Platinum Surface. *Thin Solid Films* **2009**, *517* (9), 2871–2877.

(6) Solla-Gullón, J.; Vidal-Iglesias, F. J.; López-Cudero, A.; Garnier, E.; Feliu, J. M.; Aldaz, A. Shape-Dependent Electrocatalysis: Methanol and Formic Acid Electrooxidation on Preferentially Oriented Pt Nanoparticles. *Phys. Chem. Chem. Phys.* **2008**, *10* (25), 3689.

(7) Santiago, L.; Sanchez-Pomales, G.; Rios-Pagan, A.; Cabrera, C. R. Electrochemical Study and Preparation of Gold Substrates Functionalized with Single-Walled Carbon Nanotubes for DNA Biosensor Application. *ECS Trans.* **2007**, *3* (28), 15–26.

(8) Sánchez-Pomales, G.; Santiago-Rodríguez, L.; Rivera-Vélez, N. E.; Cabrera, C. R. Control of DNA Self-Assembled Monolayers Surface Coverage by Electrochemical Desorption. *J. Electroanal. Chem.* **2007**, *611* (1–2), 80–86.

(9) Kakiuchi, T.; Usui, H.; Hobara, D.; Yamamoto, M. Voltammetric Properties of the Reductive Desorption of Alkanethiol Self-Assembled Monolayers from a Metal Surface. *Langmuir* **2002**, *18* (13), 5231–5238.

(10) Sánchez-Pomales, G.; Cabrera, C. R. Vertical Attachment of DNA–CNT Hybrids on Gold. *J. Electroanal. Chem.* **2007**, *606* (1), 47–54.

(11) Huffman, M. L.; Venton, B. J. Electrochemical Properties of Different Carbon-Fiber Microelectrodes Using Fast-Scan Cyclic Voltammetry. *Electroanalysis* **2008**, *20* (22), 2422–2428.

(12) Kuphal, M.; Mills, C. A.; Korri-Youssoufi, H.; Samitier, J. Polymer-Based Technology Platform for Robust Electrochemical Sensing Using Gold Microelectrodes. *Sensors Actuators, B Chem.* **2012**, *161* (1), 279–284.

(13) Mendonsa, S. D.; Bowser, M. T. In Vitro Selection of Aptamers with Affinity for Neuropeptide Y Using Capillary Electrophoresis. *J. Am. Chem. Soc.* **2005**, *127* (26), 9382–9383.

(14) Sanghavi, B. J.; Varhue, W.; Chávez, J. L.; Chou, C. F.; Swami, N. S. Electrokinetic Preconcentration and Detection of Neuropeptides at Patterned Graphene-Modified Electrodes in a Nanochannel. *Anal. Chem.* **2014**, *86* (9), 4120–4125.